THE JOURNAL OF PHYSICAL CHEMISTRY A

Article

pubs.acs.org/JPCA

Shock Wave Study of the Thermal Dissociations of C_3F_6 and c-C_3F_6. II. Dissociation of Hexafluorocyclopropane and Dimerization of CF_2

C. J. Cobos,[†] L. Sölter,[‡] E. Tellbach,[‡] and J. Troe*[,‡,§]

[†]INIFTA, Facultad de Ciencias Exactas, Universidad Nacional de La Plata, La Plata, Argentina

[‡]Institut für Physikalische Chemie, Universität Göttingen, Tammannstrasse 6, D-37077 Göttingen, Germany

[§]Max-Planck-Institut für Biophysikalische Chemie, Am Fassberg 11, D-37077 Göttingen, Germany

ABSTRACT: The thermal dissociation of c-C_3F_6 has been studied in shock waves over the range 620−1030 K monitoring the UV absorption of CF_2. The reaction was studied close to its high-pressure limit, but some high-temperature falloff was accounted for. Quantum-chemical and kinetic modeling rationalized the experimental data. The reaction is suggested to involve the 1,3 biradical $CF_2CF_2CF_2$ intermediate. CF_2 formed by the dissociation of c-C_3F_6 dimerizes to C_2F_4. The measured rate of this reaction is also found to correspond to the falloff range. Rate constants for $2CF_2 \rightarrow C_2F_4$ as a function of temperature and bath gas concentration [Ar] are given and shown to be consistent with literature values for the high-pressure rate constants from experiments at lower temperatures and dissociation rate constants obtained in the falloff range at higher temperatures. The onset of falloff at intermediate temperatures is analyzed.

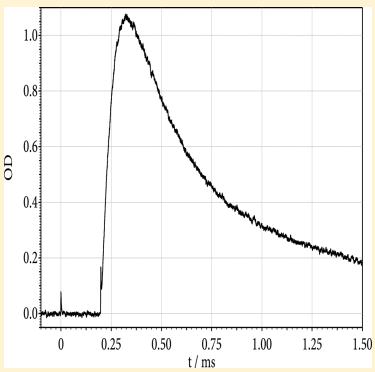

1. INTRODUCTION

The mechanism of the thermal dissociation of perfluorocyclopropane (c-C_3F_6)

$$\text{c-}C_3F_6(+M) \rightarrow C_2F_4 + CF_2(+M) \qquad \Delta H_0^\circ \approx 36.6\ \text{kcal mol}^{-1} \tag{1}$$

has found considerable attention. Although there has only been a single experimental study[1] over a small temperature range (526−549 K), several theoretical investigations[2−5] have been undertaken to clarify pathway and energetics. In spite of these efforts, the conclusions still are controversial; see the discussion in ref 6. The quantum-chemical calculations of ref 5 indicated a single transition state at 49.6 kcal mol^{-1}. In addition, these calculations led to a single transition state at 62.6 kcal mol^{-1} for the isomerization

$$\text{c-}C_3F_6 \rightarrow C_3F_6 \qquad \Delta H_0^\circ \approx -31.3\ \text{kcal mol}^{-1} \tag{2}$$

(for reaction enthalpies, see Appendix of part I of this series[7]). Contrary to these results, the earlier quantum-chemical calculations from refs 2 and 3 found a pathway with two transition states, passing through a $CF_2CF_2CF_2$ 1,3 biradical (the "bond-stretched invertomer" of c-C_3F_6, see ref 4). Likewise, two transition states enclosing $CF_2CF_2CF_2$ were detected on the way from C_3F_6 to $CF_2 + C_2F_4$, i.e., for the reaction

$$C_3F_6(+M) \rightarrow C_2F_4 + CF_2(+M) \qquad \Delta H_0^\circ = 67.9\ \text{kcal mol}^{-1} \tag{3}$$

which again was in contrast to the findings of ref 5.

In part I of this series,[7] we studied the thermal dissociation of C_3F_6 (3) in detail both experimentally and theoretically. At the temperatures employed (T > 1300 K), the dissociation was found to proceed by bond fission processes. We showed that the rigid activated complex process (3) only dominates the reaction at temperatures below about 1100 K. As we confirmed the conclusions of ref 3 for the energy profile or reaction 3, it appeared logical to extend our work also to reaction 1. This is the issue of the present article. We again performed quantum-chemical calculations in addition to experimental work, the latter markedly extending the experimental temperature range (620−1030 K). Analyzing our experimental results by kinetic modeling, we concluded that the data correspond to a unimolecular reaction close to its high-pressure limit, although some falloff corrections had to be applied at the highest temperatures. As in part I, we proceeded to a representation of the full temperature and pressure dependence of the rate constant k_1 (also estimating some falloff corrections for the results of ref 1). Our quantum-chemical calculations clearly indicated the importance of $CF_2CF_2CF_2$ along the path of the reaction, in agreement with refs 3 and 4 but opposite to the conclusions of ref 5.

While our study is only the second experimental investigation of the dissociation of c-C_3F_6, there have been quite a few[1,5,8−13] on the addition of CF_2 to C_2F_4. While the pathway

Received: February 13, 2014
Revised: June 6, 2014

   dx.doi.org/10.1021/jp501577k | J. Phys. Chem. A XXXX, XXX, XXX−XXX

$$C_2F_4 + CF_2(+M) \rightarrow c\text{-}C_3F_6(+M) \qquad \Delta H_0^\circ \approx -36.6\ \text{kcal mol}^{-1} \tag{4}$$

was considered as dominant,[5,8−10] the possibility of a reaction

$$C_2F_4 + CF_2(+M) \rightarrow C_3F_6(+M) \qquad \Delta H_0^\circ = -67.9\ \text{kcal mol}^{-1} \tag{5}$$

has also been discussed.[11−13] This aspect of the reaction system has been considered in part I of this series.[7] We note that reactions 4 and 5 were included in the modeling of larger reaction mechanisms such as presented in refs 5 and 14−16, while reaction 1 generally was omitted.

The thermal dissociation of c-C_3F_6 is an excellent source of CF_2 at temperatures below those where CF_2 is formed by thermal dissociation of C_2F_4, i.e., by

$$C_2F_4(+M) \rightarrow 2CF_2(+M) \qquad \Delta H_0^\circ = 67.5\ \text{kcal mol}^{-1} \tag{6}$$

In a previous article[17] we studied this reaction, also monitoring CF_2 formation (the reaction enthalpy is from this work). An important additional aspect of the present article thus is the possibility to access the dimerization of CF_2

$$2CF_2(+M) \rightarrow C_2F_4(+M) \qquad \Delta H_0^\circ = -67.5\text{kcal mol}^{-1} \tag{7}$$

In this way, we can fill the gap between low-temperature studies of reaction 7 reaching up to[18] 873 K and studies of the reverse reaction 6 reaching down to 1100 K as described in ref 17. Particular emphasis in our work again has been put on the pressure dependence of reactions 6 and 7. Falloff effects in all of the reactions 1−7 so far have been neglected in modelings of larger reaction systems. In some instances this has led to erroneous conclusions about the primary reaction products (see, e.g., the analogous discussion of the dissociations of C_2F_5H and C_3F_7H in ref 19). Our observation of reaction 7 took advantage of the recalibration of the UV absorption coefficients of CF_2 reported in ref 17. By monitoring CF_2 absorption−time profiles, not only primary dissociations but also secondary reactions could be followed, see, e.g., refs 17 and 19−22. The present study exploits this opportunity in particular detail by measuring the rate of reaction 7. In addition, the rate constant for reaction 1 could be determined sensitively over a wide range of reactant concentrations.

2. EXPERIMENTAL TECHNIQUE AND RESULTS

Analogous to our previous work,[7,17,19−22] we monitored the formation and consumption of CF_2 in the dissociation of c-C_3F_6 behind incident and reflected shock waves. The wavelength for observing the UV absorption of CF_2 was 248 nm. Details of our shock wave technique do not have to be described again (see refs 7, 17, 19−22). We varied the concentration of the reactant (purity >99%, from abcr) in the bath gas argon (purity >99.9999%, from Air Liquide) between about 70 and 4000 ppm. The experimental temperatures were varied between 620 and 1030 K while [Ar] was between 3×10^{-5} and 7×10^{-5} mol cm^{-3}.

Figures 1−3 illustrate the variety of observed CF_2 absorption−time profiles. Quite clearly the profiles of CF_2 were dominated by reactions 1 and 7 only. In part, the variation of the signals is due to the difference in the temperature coefficients of reactions 1 and 7. Furthermore, reaction 1 is a first-order process with respect to the reactant concentration while reaction 7 is a second-order process such that the relative time scales could be varied by changes of the reactant concentration. Figure 1 shows an example at higher temperatures (1023 K) with high (2000 ppm) reactant concentration and under conditions where reaction 1 is markedly faster than reaction 7. The CF_2 yield was always found to correspond to

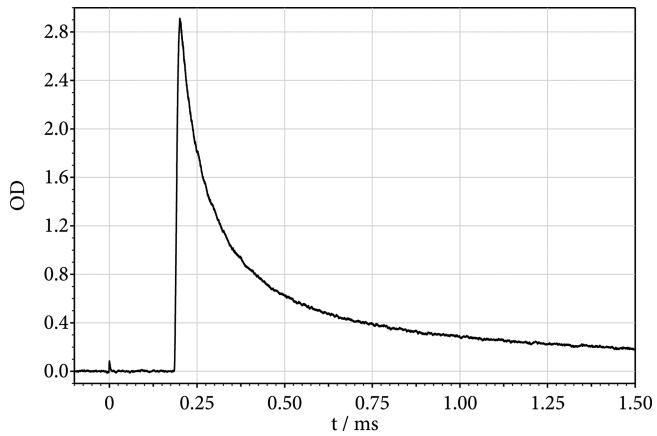

Figure 1. Absorption−time profile (at 248 nm) of CF_2 after formation in the dissociation of c-C_3F_6 at 1022 K and [Ar] = 5.7×10^{-5} mol cm^{-3} (initial reactant concentration of c-C_3F_6 = 2000 ppm in Ar).

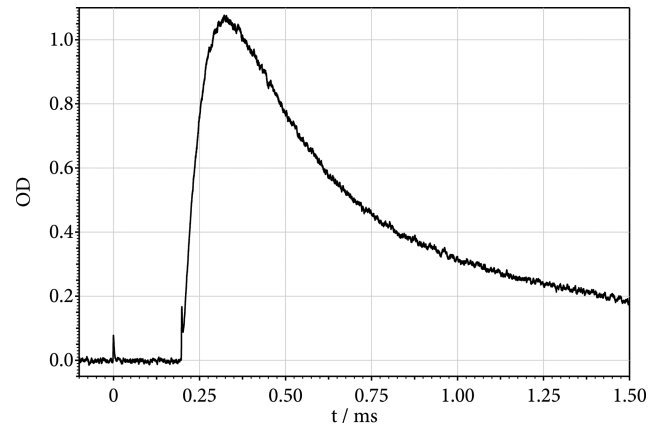

Figure 2. As Figure 1: formation and consumption of CF_2 in the dissociation of c-C_3F_6 at 858 K and [Ar] = 6.8×10^{-5} mol cm^{-3} (initial reactant concentration 2000 ppm in Ar).

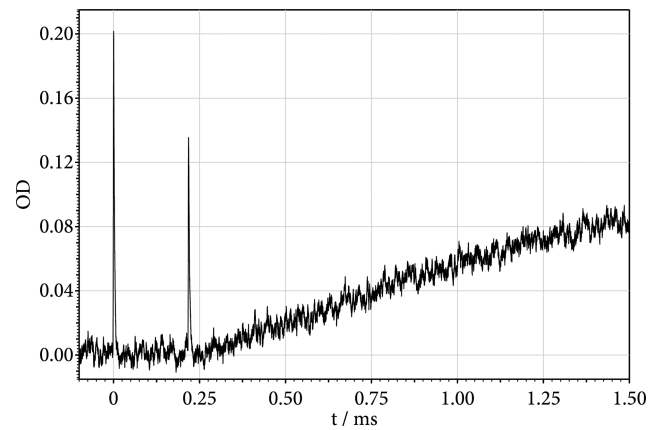

Figure 3. As Figure 1: formation of CF_2 in the dissociation of c-C_3F_6 at 784 K and [Ar] = 5.9×10^{-5} mol cm^{-3} (initial reactant concentration 2000 ppm in Ar).

one CF_2 formed per one c-C_3F_6 decomposed. The CF_2 yield was determined both from the initial reactant concentration and from the absorption of CF_2 with the absorption coefficient from ref 17. Figure 1 illustrates well the hyperbolic second-order time law of CF_2 disappearance due to reaction 7. At medium temperatures, the time scales for CF_2 formation and consumption are less well separated such as illustrated in Figure 2 (for T = 858 K). At even lower temperatures, CF_2 formation becomes so slow that it finally is not complete during our observation time of about 1 ms. This is illustrated in Figure 3 (for T = 680 K). With our lowest temperatures (near 620 K), almost the temperature range covered by ref 1 (526−549 K) was reached. Examples of measured rate constants k_1 and experimental conditions are given in Table 1.

Table 1. Examples of Rate Constants k_1

T/K	[Ar]/mol cm^{-3}	[c-C_3F_6]$_0$/[Ar]	k_1/s^{-1}	$k_{1,\infty}$/s^{-1}
627	4.2×10^{-5}	2000	1.1×10^{0}	1.1×10^{0}
644	3.9×10^{-5}	2000	2.1×10^{0}	2.2×10^{0}
659	3.7×10^{-5}	3800	9.6×10^{0}	1.0×10^{1}
680	3.6×10^{-5}	2000	1.2×10^{1}	1.3×10^{1}
709	3.4×10^{-5}	2000	4.9×10^{1}	5.5×10^{1}
765	4.32×10^{-5}	70	3.7×10^{2}	4.4×10^{2}
794	4.6×10^{-5}	80	9.5×10^{2}	1.2×10^{3}
877	3.7×10^{-5}	570	1.1×10^{4}	1.6×10^{4}
929	3.3×10^{-5}	570	2.9×10^{4}	4.4×10^{4}
994	2.9×10^{-5}	520	7.1×10^{4}	1.3×10^{5}
1025	2.7×10^{-5}	520	1.9×10^{5}	3.5×10^{5}

Figure 4 shows an Arrhenius representation of k_1. Within the scatter no dependence of k_1 on [c-C_3F_6]$_{t=0}$/[Ar] was noticed.

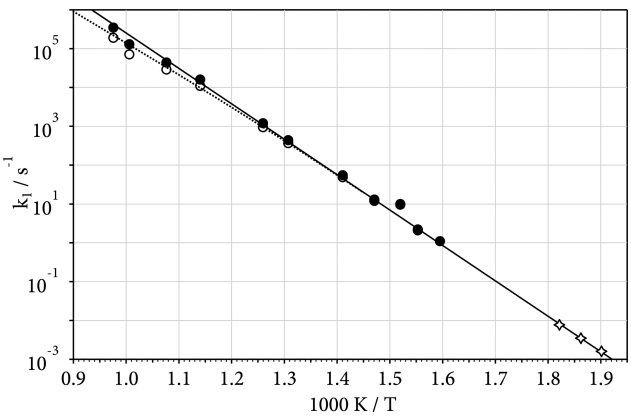

Figure 4. Rate constants k_1 for the thermal dissociation of c-C_3F_6 (○) measurements at [Ar] = (3−6) × 10^{-5} mol cm^{-3}, (●) $k_{1,\infty}$ after falloff correction of the points ○; (full line) $k_{1,\infty}$ of eq 10, (dashed line) k_1 ([Ar] = 4 × 10^{-5} mol cm^{-3}); (◇) measurements of ref 1).

The modeling of the falloff curves given below, however, shows that our measured k_1 near 1000 K were about a factor of 2, near 800 K a factor of 1.3, and near 650 a factor of 1.07 below the limiting high pressure rate constant $k_{1,\infty}$. Therefore, Figure 4 includes modeled representations of k_1(T) at fixed [Ar] = 4 × 10^{-5} mol cm^{-3} together with the deduced limiting high pressure rate constants $k_{1,\infty}$. The experiments of ref 1, at a pressure of 20−160 Torr, were also not done completely at the high pressure limit (for 20 Torr, $k_1/k_{1,\infty} \approx 0.6$ is estimated and, for 160 Torr, about $k_1/k_{1,\infty} \approx 0.85$; as individual conditions were not specified in ref 1, falloff corrections could not be applied). Our modeling of the falloff curves allows for a complete representation of the temperature- and pressure-dependence of k_1, see below. By means of this, the present experiments and the results from ref 1 can be located on the falloff curves.

It should be mentioned that the reactant concentrations in our work were always so low that, unlike ref 1, reactions 4 and 5 between CF_2 and C_2F_4 were far too slow to be of importance (see rate constants in refs 1, 5, and 7−13). Table 2 summarizes results for the rate constant k_7. While k_1 strongly increases with increasing temperature, our values of k_7 apparently are temperature independent. The small accessible range of [Ar] concentrations prevented us from detecting a pressure dependence of k_7. However, the detailed modeling of k_7 given below explains why k_7 does not follow the positive temperature dependence observed for the limiting high-pressure rate constant $k_{7,\infty}$. At constant [Ar], with increasing temperature k_7 increasingly falls below $k_{7,\infty}$ which compensates the increase of $k_{7,\infty}$. These effects are illustrated in more detail below.

Table 2. Examples of Rate Constants k_7

T/K	[Ar]/mol cm^{-3}	[c-C_3F_6]$_0$/[Ar]	k_7/cm^{-3} mol^{-1} s^{-1}
842	7.0×10^{-5}	900	7.8×10^{10}
858	6.8×10^{-5}	900	8.1×10^{10}
870	7.2×10^{-5}	70	1.1×10^{11}
884	7.0×10^{-5}	70	9.1×10^{10}
896	4.4×10^{-5}	3800	7.3×10^{10}
898	6.7×10^{-5}	900	8.3×10^{10}
910	6.5×10^{-5}	520	1.0×10^{11}
940	6.1×10^{-5}	900	7.9×10^{10}
944	4.1×10^{-5}	3800	8.0×10^{10}
994	2.9×10^{-5}	520	8.4×10^{10}
1020	5.7×10^{-5}	2000	7.4×10^{10}
1020	5.6×10^{-5}	900	7.4×10^{10}
1022	5.7×10^{-5}	2000	9.6×10^{10}

3. QUANTUM-CHEMICAL CALCULATION OF ENERGY PROFILES

We have calculated the minimum-energy path (MEP) and the energetics of reaction 1 with its intermediate transition states by several quantum-chemical methods. We employed the CBS-QB3 method from ref 24, the G4 method from ref 25, and the reduced G4MP2 version of G4 from ref 26, carrying out all calculations on the Gaussian 09 software[27] (details of our quantum-chemical calculations are given in the Appendix of part I of this series[7] together with a discussion of their reliability and structures of the transition states TS1, TS2, and $CF_2CF_2CF_2$). Figure 5 shows the MEP energy profile as obtained from G4 calculations and Table 3 compares the results from the different methods for different parts of the intrinsic reaction mechanism (Figure 5 corresponds to Figure 11 from the discussion in ref 6, based on the calculations from ref 4 which placed $CF_2CF_2CF_2$ about 20.7 kcal mol^{-1} above c-C_3F_6).

The energetics of Figure 5 suggests that reaction 1 is governed by the overcoming of TS2 whose vibrational frequencies and rotational constants in our work were determined by B3LYP/6-31G(2df,p) calculations as given in the Appendix. The calculated energy barrier TS2 of 7.0 kcal mol^{-1} for the formation of $CF_2CF_2CF_2$ from CF_2 + C_2F_4 corresponds well to the experimental temperature coefficient of

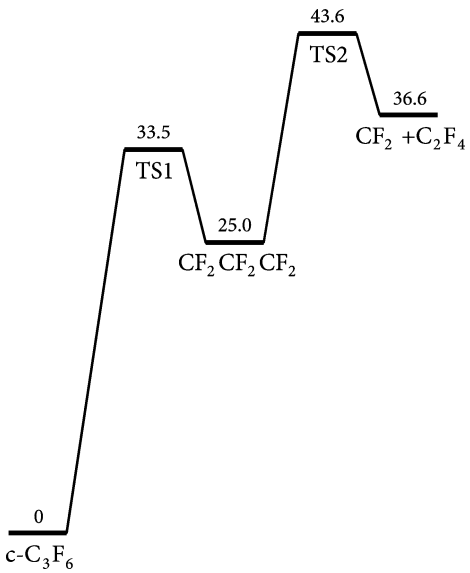

Figure 5. Minimum-energy path for the dissociation of c-C_3F_6 (energies in kcal mol^{-1}; G4 calculations of the present work, see section 3).

Table 3. Calculated Reaction Enthalpies and Enthalpies of Transition States (at 0 K, in kcal mol^{-1}, See Text)

reaction	CBS-QB3[24]	G4MP2[26]	G4[25]
c-C_3F_6 → CF_2 + C_2F_4 (1)	38.4	35.5	36.6
c-C_3F_6 → $CF_2CF_2CF_2^{\ddagger}$ (TS1)	38.8	33.0	33.5
$CF_2CF_2CF_2^{\ddagger}$ (TS1) → $CF_2CF_2CF_2$	−13.5	−9.4	−8.5
$CF_2CF_2CF_2$ → C_2F_4−$CF_2^{\ddagger}$ (TS2)	19.5	19.5	18.6
C_2F_4−$CF_2^{\ddagger}$ (TS2) → C_2F_4 + CF_2	−6.5	−7.7	−7.0
c-C_3F_6 → C_2F_4−$CF_2^{\ddagger}$ (TS2)	44.8	43.1	43.6

the combination of CF_2 with C_2F_4, see below. On the other hand, the calculated energy barrier TS1 of 8.5 kcal mol^{-1} for the isomerization of $CF_2CF_2CF_2$ to c-C_3F_6 is much smaller than the calculated barrier of 29.9 kcal mol^{-1} for the isomerization of $CF_2CF_2CF_2$ to C_3F_6, see part I.[7] This favors reaction 4 over reaction 5, see below. Having in hands energetics and transition state parameters of TS2, one can proceed to a modeling of k_1 and its temperature and pressure dependence. The results of this kinetic modeling are described in the following section.

4. TEMPERATURE AND PRESSURE DEPENDENCES OF REACTIONS 1 AND 7

The temperature and pressure dependence of k_7 has been modeled before in refs 17 and 23 and needs not to be described again. The following parameters characterizing the falloff curve were derived: $k_{7,0}$ = [Ar]4.40 × $10^{21}(T/300\ \mathrm{K})^{-6.7}$ cm^6 mol^{-2} s^{-1} (over the temperature range 1200−1600 K), $k_{7,\infty}$ = 2.26 × $10^{10}(T/300\ \mathrm{K})^{1.53}$ cm^3 mol^{-1} s^{-1}, and F_{cent} = 0.91 exp(−T/250 K) + 0.09 exp(−T/12 500 K) + exp(−7400 K/T). With these quantities, k_7 is represented employing the expression recommended in ref 23, i.e., $k_7/k_{7,\infty} = [x/(1 + x)]F(x)$, where $x = k_{7,0}/k_{7,\infty}$ and the broadening factor $F(x)$ is given by

$$F(x) \approx (1 + x)/[1 + x^n]^{1/n} \quad (8)$$

with $n = [\ln 2/\ln(2/F_{cent})][0.8 + 0.2x^q]$ and $q = (F_{cent} - 1)/\ln(F_{cent}/10)$. Figure 6 first shows curves of $k_7(T)$ for fixed bath gas concentrations as modeled with these input data and eq 8.

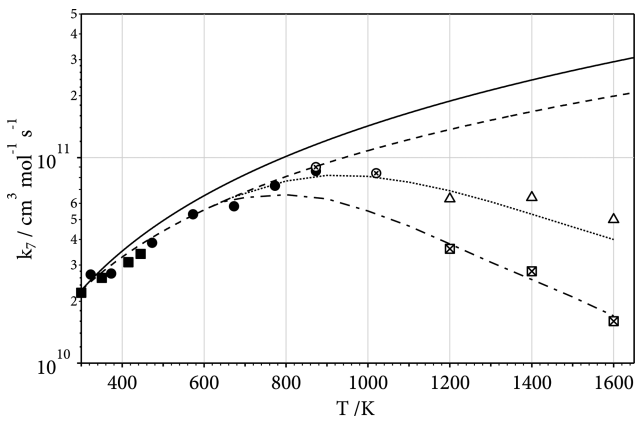

Figure 6. Rate constants k_7 for the dimerization $2CF_2$(+Ar) → C_2F_4(+Ar) ((full line) $k_{7,\infty}$ from modeling of ref 17; (dashed line) $k_{7,\infty}$ after modification in the present work; (dotted curve) k_7([Ar] = 5 × 10^{-5} mol cm^{-3}) from present modeling; (dash-dotted curve) k_7([Ar] = 1 × 10^{-5} mol cm^{-3}) from present modeling; (△,cross in square) from dissociation experiments of ref 17; (⊗) present experiments at [Ar] = 5 × 10^{-5} mol cm^{-3}; (●) ref 18, at 1 bar of Ar; (■) ref 9, at 50 Torr of N_2).

The figure includes data from direct measurements of k_7 at lower temperatures and data from dissociation experiments[17,23] converted with the equilibrium constant[17] $K_c = k_6/k_7$ = 7.56 × $10^5(T/300\ \mathrm{K})^{-2.4}$ exp(−35 050 K/T) mol cm^{-3}. The value for $k_{7,\infty}$ given above is from the ab initio modeling of ref 17 which already showed remarkable agreement with the experiments. In order to further improve this agreement, we further fine-tuned $k_{7,\infty}$ empirically and finally used

$$k_{7,\infty} = 2.26 \times 10^{10}(T/300\,\mathrm{K})^{1.3}\ \mathrm{cm^3\ mol^{-1}\ s^{-1}} \quad (9)$$

(dashed line in Figure 6). Figure 6 explains why k_7 from the present work shows practically no temperature dependence. While pressure dependences of k_7 are less important in low-temperature experiments they have to be accounted for at higher temperatures. This is illustrated in Figure 7 where, for fixed T, $k_7(P)$ is illustrated. The usual marked shift of the falloff

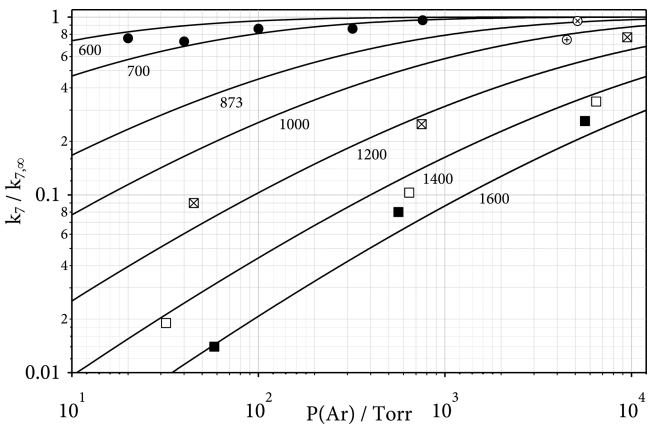

Figure 7. Falloff curves $k_7/k_{7,\infty}$ for the dimerization of CF_2 in Ar (modeled curves from top to bottom for 700, 873, 1000, 12 000, 1400, and 1600 K: (●) experiments from ref 18 at 873 K, (⊗) present experiments at 873 K, (⊕) present experiments at 1000 K, (cross in square) $k_7/k_{7,\infty}$ from ref 17 at 1200 K, (□) k_7/ $k_{7,\infty}$ from ref 17 at 1400 K, (■) $k_7/k_{7,\infty}$ from ref 17 at 1600 K with modified $k_{7,\infty}$ from present work).

curves with temperature becomes quite apparent. We again[17] note that the pressure dependence of ref 18 at 873 K, for unknown reasons, unfortunately cannot be reconciled with the present modeling.

Falloff curves for reaction 1 have not been considered before. In this case, we first estimated the low-pressure rate constant $k_{1,0}$ following ref 28. We then determined doubly reduced falloff curves $k_1/k_{1,\infty}$ as a function of $x = k_{1,0}/k_{1,\infty}$ as described by eq 8. In order to estimate $F_{cent,1}$, the method of ref 29 was employed using the transition-state parameters as given in the Appendix. Again, broad falloff curves with $F_{cent,1}$ = 0.08 (±0.005) are expected over the range 550−1000 K. By the reduced falloff curves then the falloff corrections $k_1/k_{1,\infty}$ for the present experiments were estimated which finally led to $k_{1,\infty}$ such as given in Table 1 and shown in Figure 4. We note that $k_{1,\infty}$ from the present work and from ref 1 as determined in this way are consistent. A combination of the derived values from ref 1 and the present work leads to

$$k_{1,\infty} = 3.3 \times 10^{14} \exp(-21000\ \mathrm{K}/T)\ \mathrm{s}^{-1} \tag{10}$$

In the modeling of reduced falloff curves, a low-pressure rate constant of

$$k_{1,0} \approx [\mathrm{Ar}]1.76 \times 10^{23}(T/300\ \mathrm{K})^{-6.5} \exp(-18420\ \mathrm{K}/T)\ \mathrm{cm}^3\ \mathrm{mol}^{-1}\ \mathrm{s}^{-1} \tag{11}$$

was employed while $F_{cent,1}$ was taken as 0.08 (±0.005). As the falloff corrections were comparably small, a further fine-tuning of $k_{1,0}$ was not required.

5. RATE CONSTANTS OF THE REACTION $C_2F_4 + CF_2 \rightarrow$ c-C_3F_6

Because of the very broad falloff curves of k_1, due to the small value of F_{cent}, pressure dependences of the measured k_1 in the present work and in ref 1 within the experimental scatter could not be detected. Nevertheless, as the modeling of section 4 showed, they are there and may have to be taken into account. That applies also to some of the measurements of k_4 in refs 8−10. While the measurements near 300 K from refs 8 and 9 undoubtedly corresponded to $k_{4,\infty}$, some minor falloff had to be considered for k_4 at 500 K (less for the measurements of ref 10 which were done at 1 bar and more for the measurements of ref 8 at less than 60 Torr). Figure 8 compares experimental values for $k_{4,\infty}$. The plot shows a positive temperature coefficient of $k_{4,\infty}$ which is a consequence of the energy barrier illustrated in Figure 5. All results from refs 1 and 8−10 corresponded to measurements of the ratio $k_4/k_7^{1/2}$ and were corrected with the present $k_{7,\infty}$. While the data of refs 1 and 10 nearly agree, there is some discrepancy between these and data from refs 8 and 9.

In the following, we exploit the combined results from Figures 4 and 8 in two ways: first, we derive an experimental equilibrium constant $K_{c,1} = k_1/k_4$ in order to compare quantum-chemical with experimental thermochemical values; second, we compare the experimental $k_{1,\infty}$ and $k_{4,\infty}$ with modeled values in order to fine tune the quantum-chemical results for the barrier between $CF_2CF_2CF_2$ and $C_2F_4 + CF_2$. $k_{4,\infty}(500\ \mathrm{K}) = 7.2 \times 10^6$ $\mathrm{cm}^3\ \mathrm{mol}^{-1}\ \mathrm{s}^{-1}$ was measured in ref 10 with an uncertainty of about a factor of 2, while $k_{4,\infty}(500\ \mathrm{K}) = 4.0 \times 10^6\ \mathrm{cm}^3\ \mathrm{mol}^{-1}\ \mathrm{s}^{-1}$ after falloff correction follows from ref 8. With $k_{1,\infty}(500\ \mathrm{K}) = 1.9 \times 10^{-4}\ \mathrm{s}^{-1}$ from eq 10 and using $k_{4,\infty}$ from ref 10, this leads to $K_{c,1}(500\ \mathrm{K}) = k_{1,\infty}/k_{4,\infty} = 2.6 \times 10^{-11}\ \mathrm{mol\ cm}^{-3}$ with an uncertainty of about a factor of 2. Modeling with G4 energies and frequencies from the Appendix would have given

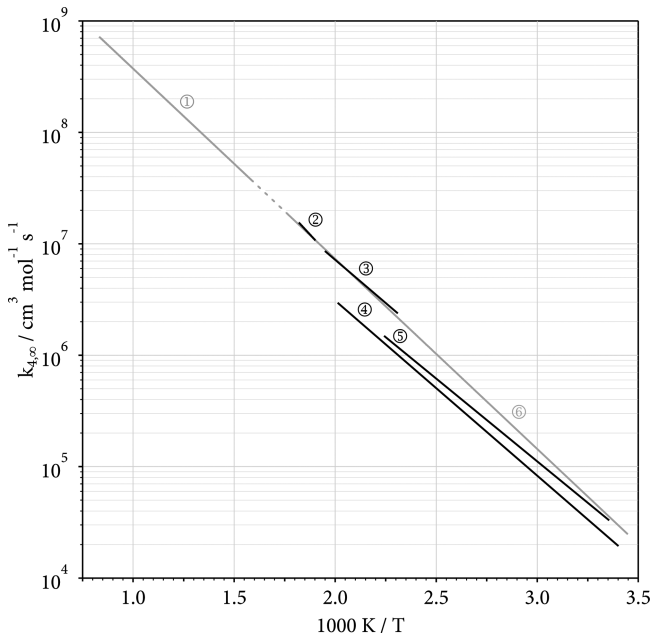

Figure 8. High-pressure rate constants $k_{4,\infty}$ for the reaction $CF_2 + C_2F_4 \rightarrow$ c-C_3F_6: 1, present work; 2, ref 1; 3, ref 10; 4, ref 8; 5, ref 9; 1 and 6, eq 14 of the present work; data of refs 8−10 reevaluated with $k_{7,\infty}$ from the present work.

$K_{c,1} = 1.74 \times 10^4 \exp(-17\,690\ \mathrm{K}/T)$ mol cm^{-3} and hence $K_{c,1}(500\ \mathrm{K}) = 7.5 \times 10^{-12}$ mol cm^{-3}. Reducing the reaction enthalpy (at 0 K) from 36.6 to 36.1 kcal mol^{-1} while keeping the preexponential factor (corresponding to a third-law analysis) brings agreement with the experimental K_c (a factor of 2 uncertainty corresponding to an uncertainty of the enthalpy of about 0.7 kcal mol^{-1}). As the enthalpies of formation of C_2F_4 and CF_2 now appear well established, being $\Delta H_{f,0}°(C_2F_4) = -160.6$ kcal mol^{-1} and $\Delta H_{f,0}°(CF_2) = -46.6$ kcal mol^{-1} (see refs 17, 29, and 30), an experimental reaction enthalpy of 36.1 (±0.7) kcal mol^{-1} from the above analysis would correspond to $\Delta H_{f,0}°(\text{c-}C_3F_6) = -243.2$ (±0.7) kcal mol^{-1} which is in very good agreement with the G4 value of the present work of −243.8 kcal mol^{-1}. This is also in very good agreement with the earlier G3MP2 value of −244.5 kcal mol^{-1} of ref 31. The present experimental value, therefore, now is in better agreement with quantum-chemical values than the collection of earlier experimental values from ref 6 which led to an experimental value of about $\Delta H_{f,0}°(\text{c-}C_3F_6) = -232.2$ kcal mol^{-1}. On the basis of this discussion, we recommend

$$K_{c,1} = 1.7 \times 10^4 \exp(-17070\ \mathrm{K}/T)\ \mathrm{mol\ cm}^{-3} \tag{12}$$

We finally compare our measured $k_{1,\infty}$ with modeled values based on the energetics of Figure 5 and the transition state (TS2) parameters from the Appendix. This leads to

$$k_{1,\infty} = 2.7 \times 10^{14}(T/300\ \mathrm{K})^{1.18} \exp(-21940\ \mathrm{K}/T)\ \mathrm{s}^{-1} \tag{13}$$

Comparing eqs 10 and 13, we observe that the modeled value of $k_{1,\infty}$ at 1000 K is about a factor of 1.3 smaller than the experimental value which can be considered as good agreement. Combining $k_{1,\infty}$ from eq 13 with $K_{c,1}$ from eq 12, leads to a recommended value of $k_{4,\infty}$ of

Table 4. Summary of Preferred Rate Constants (To Be Used in the Falloff Expression of Eq 8, See the Text)

reaction		note
1	$k_{1,0} \approx [\mathrm{Ar}]1.8 \times 10^{23}(T/300\ \mathrm{K})^{-6.5} \exp(-18420\ \mathrm{K}/T)\ \mathrm{cm^3\ mol^{-1}\ s^{-1}}$	eq 11
	$k_{1,\infty} \approx 3.3 \times 10^{14} \exp(-21000\ \mathrm{K}/T)\ \mathrm{s^{-1}}$	eq 10
	$F_{\mathrm{cent},1} \approx 0.08$	500−1000 K
4	$k_{4,0} \approx [\mathrm{Ar}]1.0 \times 10^{19}(T/300\ \mathrm{K})^{-6.5} \exp(-1350\ \mathrm{K}/T)\ \mathrm{cm^6\ mol^{-2}\ s^{-1}}$	eqs 11, 12
	$k_{4,\infty} \approx 1.9 \times 10^{10} \exp(-3930\ \mathrm{K}/T)\ \mathrm{cm^3\ mol^{-1}\ s^{-1}}$	eq 14
	$F_{\mathrm{cent},4} \approx 0.08$	500−1000 K
6	$k_{6,0} \approx [\mathrm{Ar}]1.3 \times 10^{28}(T/300\ \mathrm{K})^{-9.7} \exp(-36660\ \mathrm{K}/T)\ \mathrm{cm^3\ mol^{-1}\ s^{-1}}$	ref 17
	$k_{6,\infty} \approx 1.7 \times 10^{16} \exp(-35050\ \mathrm{K}/T)\ \mathrm{s^{-1}}$	eq 9, ref 17.
	$F_{\mathrm{cent},6} \approx 0.1$	ref 23
7	$k_{7,0} \approx [\mathrm{Ar}]4.4 \times 10^{21}(T/300\ \mathrm{K})^{-6.7}\ \mathrm{cm^6\ mol^{-2}\ s^{-1}}$	ref 17
	$k_{7,\infty} \approx 2.26 \times 10^{10}(T/300\ \mathrm{K})^{-1.3}\ \mathrm{cm^3\ mol^{-1}\ s^{-1}}$	eq 9
	$F_{\mathrm{cent},7} \approx 0.1$	ref 23

$$k_{4,\infty} = k_{1,\infty}/K_{c,1} = 1.9 \times 10^{10} \exp(-3930\ \mathrm{K}/T)\ \mathrm{cm^3\ mol^{-1}\ s^{-1}} \quad (14)$$

Figure 8 includes this expression which agrees well with the data from refs 1 and 10 which, therefore, are preferred here.

6. CONCLUSIONS

The thermal decomposition of cyclo-C_3F_6 through reaction 1 can be studied in shock waves conveniently by monitoring the UV absorption of CF_2. We found that falloff effects have to be taken into account such that not only the temperature but also the pressure dependence of the reaction needs to be accounted for. Equation 10 represents the limiting high-pressure rate constant $k_{1,\infty}$ over the range 500−1100 K; the modeled low-pressure rate constant $k_{1,0}$ from eq 11 together with a modeled center broadening factor $F_{\mathrm{cent}} \approx 0.08$ and falloff expressions of eq 8 then allows one to characterize the full pressure and temperature dependence of k_1. The combination with the equilibrium constant $K_{c,1}$ of eq 12 leads to rate constants of the reverse reaction 4. The combined data set now covers the temperature range 300−1100 K. The combination of results for reactions 1 and 4 also allows one to derive the enthalpy of formation of c-C_3F_6 as $\Delta H_{f,0}°(\text{c-}C_3F_6) = -243.2\ (\pm 0.7)$ kcal mol^{-1} in agreement with the quantum-chemical values of −244 (±1) kcal mol^{-1}.

The pyrolysis of c-C_3F_6 is an excellent source for CF_2. In the present work this was used to study the combination of two CF_2 to C_2F_4 over the temperature range 840−1020 K, thus bridging the gap between previous dimerization studies at lower temperatures and the temperature range accessed in C_2F_4 dissociation experiments. We demonstrated that it is of crucial importance, besides the temperature dependence also to analyze the pressure dependence. The falloff representation of the rate constant from our earlier dissociation experiments was found to apply well again. A minor adjustment of the limiting high-pressure rate constant $k_{7,\infty}$ improved the agreement between measured and modeled rate constants over very large ranges of conditions.

In order to facilitate the use of our results, Table 4 summarizes recommended rate constants for reactions 1, 4, 6, and 7, to be employed with the falloff expression of eq 8, i.e., $k/k_\infty = [x/(1 + x)]F(x)$, where $x = k_0/k_\infty$, $F(x) \approx (1 + x)/[1 + x^n]^{1/n}$, $n = [\ln 2/\ln(2/F_{\mathrm{cent}})][0.8 + 0.2x^q]$, and $q = (F_{\mathrm{cent}} - 1)/\ln(F_{\mathrm{cent}}/10)$. Individual values for k_0, k_∞, and F_{cent} are given for each reaction. The values of F_{cent} correspond to high-temperature conditions where falloff effects become pronounced (a temperature dependence of F_{cent} thus is neglected).

■ APPENDIX: MOLECULAR PARAMETERS USED IN MODELING

(a). Harmonic Vibrational Frequencies

c-C_3F_6. ν_i/cm^{-1} = 125 (2), 178, 247 (3), 351, 495 (2), 539 (2), 731, 786, 855 (2), 1254 (2), 1267 (2), 1277, 1530; from B3LYP/6-31G(2df,p) calculations scaled by 0.9854 (from G4 model).

c-C_3F_6 → CF_2 + C_2F_4. Transition state (TS2) ν_i/cm^{-1} = 46, 108, 115, 169, 217, 295, 332, 385, 452, 521, 542, 569, 632, 784, 1092, 1126, 1194, 1321, 1366, 1700, and 335i; from B3LYP/6-31G(2df,p) calculations scaled by 0.9854 (from G4 model).

(b). Rotational Constants

c-C_3F_6. A, B, and C/cm^{-1} = 0.056, 0.056, and 0.052; from B3LYP/6-31G(2df,p) calculations (from G4 model).

c-C_3F_6 → CF_2 + C_2F_4. Transition state (TS2) A, B, and C/cm^{-1} = 0.058, 0.050, and 0.047; from B3LYP/6-31G(2df,p) calculations (from G4 model).

Data for transition state TS1 and for C_3F_6 are included in the Appendix of part I.[7]

■ AUTHOR INFORMATION

Corresponding Author

*E-mail: shoff@gwdg.de. Tel.: +49-(0)551-3933112.

Notes

The authors declare no competing financial interest.

■ ACKNOWLEDGMENTS

Support of this work by K. Hintzer, K. Luther, and A. Thaler is gratefully acknowledged.

■ REFERENCES

(1) Atkinson, B.; McKeagan, D. The Thermal Decomposition of Perfluorocyclopropane. *J. Chem. Soc., Chem. Commun.* **1966**, 189−190.

(2) Kohler, W. H.; Ritter, E. R. Pathways to Perfluoropropene: An MCSCF Investigation. Chemical and Physical Processes in Combustion (Combustion Institute, Eastern Section US, Fall Technical Meeting, 2001), p 107; results shown in refs 5 and 6.

(3) Bilera, I. V.; Borisov, Y. A.; Buravtsev, N. N.; Kolbanovsky, Y. A. Thermal Gas Phase Reactions in the 3C and 6F System: New Spectral, Kinetic and Quantum Chemical Data. *Dokl. Phys. Chem.* **2003**, *388*, 63−66.

(4) Wei, H.; Hrovat, D. A.; Dolbier, W. R.; Smart, B. E.; Borden, W. T. The "Bond-Stretched Invertomer" of Hexafluorocyclopropane−a New Type of Reactive Intermediate. *Angew. Chem., Int. Ed.* **2007**, *46*, 2666−2668.

(5) Yu, H.; Kennedy, E. M.; Ong, W.-H.; Mackie, J. C.; Han, W.; Dlugogorski, B. Z. Experimental and Kinetic Studies of Gas-Phase Pyrolysis of n-C_4F_{10}. *Ind. Eng. Chem. Res.* **2008**, *47*, 2579−2584.

(6) Poutsma, M. L. Chain Elongation During Thermolysis of Tetrafluoroethylene and Hexafluoropropylene: Modeling of Mechanistic Hypotheses and Elucidation of Data Needs. *J. Anal. Appl. Pyrol.* **2011**, *92*, 25−42.

(7) Cobos, C. J.; Sölter, L.; Tellbach, E.; Troe, J. Shock Wave Study of the Thermal Dissociations of C_3F_6 and c-C_3F_6. I. Dissociation of Hexafluoropropene. *J. Phys. Chem. A* **2014**, DOI: 10.1021/jp501569a.

(8) Cohen, N.; Heicklen, J. Mercury-Sensitized Photolysis of C_2F_4. *J. Chem. Phys.* **1965**, *43*, 871−873.

(9) Tyerman, W. J. R. Rate parameters for Reactions of Ground-State Difluorocarbene and Determination of the Absolute Intensity of the $\tilde{A}\ ^1B_1$-X $^1A_1$ Absorption Bands. *J. Chem. Soc., Faraday Trans.* **1969**, *65*, 1188−1198.

(10) Mel'nikovich, S. V.; Moin, F. B. Kinetics and Mechanism of Reaction of Difluorocarbene with Tetrafluoroethylene. *Kinet. Catal.* **1988**, *29*, 257−261.

(11) Buravtsev, N. N.; Grigor'ev, A. S.; Kolbanovsky, Y. A. Kinetics and Mechanism of Pyrolysis of Hexafluoropropylene. *Kinet. Catal.* **1989**, *30*, 13−22.

(12) Buravtsev, N. N.; Grigor'ev, A. S.; Kolbanovsky, Y. A. Kinetics of the Formation and Decomposition of Perfluorobutenes During Gas-Phase Pyrolysis of the Lower Perfluoroolefins. *Kinet. Catal.* **1989**, *30*, 386−390.

(13) Ainagos, A. F. Mechanism and Kinetics of Pyrolysis of Perfluorohexane. *Kinet. Catal.* **1991**, *32*, 720−725.

(14) Hynes, R. G.; Mackie, J. C.; Masri, A. R. Shock-Tube Study of the Pyrolysis of the Halon Replacement Molecule CF_3CHFCF_3. *J. Phys. Chem. A* **1999**, *103*, 54−61.

(15) Hynes, R. G.; Mackie, J. C.; Masri, E. R. Shock Tube Study of the Oxidation of C_3F_6 by N_2O. *J. Phys. Chem. A* **1999**, *103*, 5967−5977.

(16) Hynes, R. G.; Mackie, J. C.; Masri, A. R. A Shock Tube Kinetics Study on the Reaction of C_3F_6 and H Atoms at High Temperatures. *Proc. Combust. Inst.* **2000**, *28*, 1557−1562.

(17) Cobos, C. J.; Croce, A. E.; Luther, K.; Sölter, L.; Tellbach, E.; Troe, J. Experimental and Modeling Study of the Reaction C_2F_4 (+ M) ⇔ CF_2 + CF_2 (+ M). *J. Phys. Chem. A* **2013**, *117*, 11420−11429.

(18) Battin-Leclerc, F.; Smith, A. P.; Hayman, G. D.; Murrells, T. P. Kinetics of the Self-Reaction of CF_2 Radical and its Reaction with H_2, O_2, CH_4 and C_2H_4 over the Temperature Range 295 − 873 K. *J. Chem. Soc., Faraday Trans.* **1996**, *92*, 3305−3313.

(19) Cobos, C. J.; Croce, A. E.; Luther, K.; Troe, J. Shock Wave Study of the Thermal Decomposition of CF_2 and CF_3 Radicals. *J. Phys. Chem. A* **2010**, *114*, 4755−4761.

(20) Cobos, C. J.; Croce, A. E.; Luther, K.; Troe, J. Temperature and Pressure Dependence of the Reaction 2 CF_3 (+ M) ⇔ C_2F_6 (+ M). *J. Phys. Chem. A* **2010**, *114*, 4748−4754.

(21) Cobos, C. J.; Croce, A. E.; Luther, K.; Troe, J. Experimental and Modeling Study of the Unimolecular Thermal Decomposition of CF_3H. *Z. Phys. Chem.* **2011**, *225*, 1019−1028.

(22) Cobos, C. J.; Sölter, L.; Tellbach, E.; Troe, J. Shock Wave and Modeling Study of the Thermal Decomposition Reactions of Pentafluoroethane and 2-H-Heptafluoropropane. *Phys. Chem. Chem. Phys.* **2014**, *16*, 9797−9807.

(23) Troe, J.; Ushakov, V. G. Representation of "Broad" Falloff Curves for Dissociation and Recombination Reactions. *Z. Phys. Chem.* **2014**, *228*, 1−10.

(24) Montgomery, J. A.; Frisch, M. J.; Ochterski, J. W.; Petersson, G. A. A Complete Basis Set Model Chemistry. VI. Use of Density Functional geometries and Frequencies. *J. Chem. Phys.* **1999**, *110*, 2822−2827.

(25) Curtiss, L. A.; Redfern, P. C.; Raghavachari, K. Gaussian-4-Theory. *J. Chem. Phys.* **2007**, *126*, 084108−1−12.

(26) Curtiss, L. A.; Redfern, P. C.; Raghavachari, K. Gaussian-4-Chemistry Using Reduced Order Perturbation Theory. *J. Chem. Phys.* **2007**, *127*, 124105−1−8.

(27) Frisch, M. J.; Trucks, G. W.; Schlegel, H. B.; Scuseria, G. E.; Robb, M. A.; Cheeseman, J. R.; Scalmani, G. B.; Barone, K.; Menucci, B.; Petersson, G. A.; et al. *Gaussian 09, Revision A.02*; Gaussian Inc.: Wallingford, CT, 2009.

(28) Troe, J. Predictive Possibilities of Unimolecular Rate Theory. *J. Phys. Chem.* **1979**, *83*, 114−126.

(29) Feller, D.; Peterson, K. A.; Dixon, D. A. Ab Initio Coupled Cluster Determination of the Heats of Formation of $C_2H_2F_2$, C_2F_2, and C_2F_4. *J. Phys. Chem. A* **2011**, *115*, 1440−1451.

(30) Dixon, D. A.; Feller, D. Heats of Formation of CF_2, FCO, and CF_2O. *J. Phys. A* **1998**, *102*, 8209−8216.

(31) Bauschlicher, C. W.; Ricca, A. Heats of Formation for Cyclic C_4F_n, n = 4 − 8, and their Cations. *J. Phys. Chem. A* **2000**, *104*, 9026−9028.